[Title]

Genome-wide assays to characterize rAAV integration into human genomic DNA in vivo

[Authors]
Jaime Prout*, Jessica Von Stetina*, Gustavo Cerqueira, Madison Chasse, Huei-Mei Chen, Andrew Pla, Rachel Resendes, Danielle Sookiasian, Cagdas Tazearslan, Jason Wright#, John F. Thompson

***Co-first authors**
 # Corresponding Author

[Abstract]

Adeno-associated viral (AAV) vectors are used to treat genetic diseases, expressing therapeutic genes from both extrachromosomal episomes and payloads that integrate into the host genome. Assays were developed to evaluate HR-mediated on-target integration and the potential occurrence of off-target integration. While many studies have addressed elements of these processes, proper characterization requires long-read sequencing to ensure that integrated viral DNA is examined and not the more prevalent episomes. We used Oxford Nanopore to characterize integrated DNA and scan the whole genome for off-target integrations. These assays were applied to cell-based and in vivo models to study vectors that correct phenylketonuria (PKU), caused by loss of phenylalanine hydroxylase (*PAH*). Administration of the human-specific vector in a humanized-liver mouse xenograft model resulted in stable, nuclease-free integration into *PAH*. Because detection of rare integration events in a much larger pool of episomal DNA is subject to artifacts, careful assay validation was required. A long-read, genome-wide assay capable of detecting on- and off-target vector integrations showed no evidence of off-target integration. Artifactual false positive events were below the limit of blank. These data support rAAV as an investigational therapeutic for genetic diseases and reinforce the need for characterization of integration assays to avoid artifacts.

[Introduction]

rAAV DNA has been shown to exist in cells both chromosomally after genome integration and extra-chromosomally as an episome.[1-4] Upon entry into the cell's nucleus, the single-stranded rAAV vector genomes can either integrate into the genome via homologous recombination (HR) or be processed into extra-chromosomal episomes. If recombining, the two homology arms containing the homologous sequences integrate into the target genomic DNA, resulting in the insertion of the vector payload DNA located between the two homology arms. Non-homology-driven integration of AAV has been extensively studied at locations such as the AAVS1 site on chromosome 19.[3,5] In contrast, HR-dependent rAAV integration can occur when there is homologous sequence shared between the rAAV vector and the genome, resulting in HR-

driven, site-specific integration. For example, recent work using rAAV-mediated HR integration into the albumin locus took advantage of both the fidelity of HR integration and the high expression of albumin to drive transcription of the desired gene.[6-8]

Evidence for the integration of AAV and other viruses into the human genome has been demonstrated using a succession of increasingly robust methodologies. Wild-type AAV was found to integrate specifically into chr19 using in situ hybridization.[3,4] This finding was followed by the detection of AAV and other viral integrations by FISH,[9] plasmid rescue,[10] LAM-PCR,[11,12] nrLAM-PCR,[13] brute force NGS,[14] targeted capture,[15,16] single-cell approaches,[17,18] and a comparison of NGS-based approaches.[19] Some methods can be used across a broad range of viruses while others have significant limitations in particular situations. Methods that work well with efficiently recombining systems like retroviruses may not be feasible with less efficient systems like AAV where the high background of non-integrated viral genomes can lead to many artifacts. In addition, information gathered from each assay varies. No sequence information is generated with qPCR,[20] while other methods can produce integration junction sequence[21] or full-length integrated viral sequence data.

Cells transduced with rAAV can have hundreds to thousands of copies of episomal DNA per cell. The episomal and integrated DNA contain long stretches that are identical to each other in both the homology arms and payload. Because of the significant mismatch in copy number, episomal DNA can contaminate reads purportedly from integrated DNA. To ensure that homology arms from integrated viruses are evaluated rather than the more common episomal DNA, each sequence read should span the viral payload through the homology arm and into the unique genomic sequence adjacent to the integration event. Previous reports using short-read sequencing technology showed no additional changes to the genome,[22] but this finding requires confirmation via long-read sequencing. Additionally, multiple classes of other artifacts potentially arise during sample processing and NGS library preparation and these must be addressed when determining assay sensitivity.[23] Appropriate controls need to be included for an assay to be meaningful.

Accurate assessment of on- and off-target integration is essential because rAAV integration has been proposed as a means of achieving stable correction of genetic defects. Episomal expression of a vector containing a codon-optimized human PAH (CO-hPAH) DNA driven by a liver-specific promoter results in episomal expression and correction of phenylketonuria (PKU) in treated mice.[24] Subsequent studies showed that CO-hPAH with homology arms packaged in AAVHSC15 could induce nuclease-free, HR-mediated integration into the human *PAH* locus. These ~900 bp homology arms are locus- and species-specific and were designed to minimize potential off-target HR integration. To better characterize HR-driven rAAV integration, we have developed long-read sequencing assays to characterize all integration sites, independent of genomic location. These methods use techniques that have not been previously applied to rAAV integration.

78 **[Results]**

79 **rAAV vectors and on-target integration**

80 Assays to assess on-target integration via ddPCR and sequencing short PCR amplicons have
81 been described previously.[22] ddPCR is useful when the number of episomes is low, but it
82 becomes impractical when high doses of rAAV are administered and the ratio of episomal to
83 integrated DNA becomes excessive. The large number of episome-only droplets leads to an
84 episomal copy number that overwhelms the integration signal. When ddPCR could not be used,
85 amplicon sequencing was carried out using short-read sequencing across the integration
86 junctions. Because the sequences of both the integrated vector DNA and adjacent genomic
87 DNA are known, it is straightforward to design PCR primers that allow selective amplification of
88 the wild-type genomic DNA or the integrated DNA. However, the large excess of episomal DNA
89 and the potential presence of concatemers of variable structure[25] can introduce artifacts during
90 sample preparation and amplification. To minimize this, the amplicons must be sufficiently long
91 that there is payload DNA sequenced on one end of the homology arm and a non-viral genomic
92 DNA sequence on the other end. When quantitation is desired, amplification conditions also
93 need to be chosen such that a high level of episomal DNAs present does not differentially affect
94 the integrated/non-integrated DNA ratio. This is most easily done by making the primer
95 required to amplify both these DNAs product-limiting. With these requirements, primers have
96 been created that allow selective amplification and quantitation of both wild-type and
97 integrated DNAs.

98 Because rAAV integration is homology-dependent, different vectors must be used for
99 integration into mouse or human genomic DNA. Integration is more efficient in vivo than in
100 vitro so special models must be used to examine integration into human DNA. A relevant
101 system for assessing rAAV integration behavior is human hepatocytes that are engrafted into
102 FRG® mouse livers.[26] These mice have defective immune systems that allow the engraftment
103 and growth of human cells. The mouse hepatocytes are engineered to be sensitive to a
104 chemical challenge. In the appropriate conditions, most mouse hepatocytes die and are
105 replaced by human donor hepatocytes. While this model provides an in vivo setting, the mice
106 are not robust due to their defective immune system and do not survive as long as normal
107 mice. This makes them much more difficult to maintain. The challenges in working with this
108 model limit the experiments that can be done; but, despite the limitations, the model provides
109 insight into how the vector is likely to behave when administered to humans.

110 Three different vectors have been used for the integration experiments described here, two
111 with human homology arms but different payloads, and one with no homology arms. Vectors
112 are named by the species/presence of homology arms (hHA), whether a promoter is present
113 (LP1), and the protein product (hPAH). Some of these vectors have been described previously[22]
114 and are illustrated in Supplemental Figure 1. Mice are injected with either Formulation Buffer
115 (FB) as a control or differing concentrations of species-specific vectors at varying
116 concentrations. Figure 1 shows 3-7% integration can be achieved in human hepatocytes with

117 human homology arms as measured using the long-read PCR amplicon method previously
118 described.[22] A common genomic primer is amplified with either a payload or genomic primer
119 located beyond the homology arms and the ~1.4 kb amplicons are long-read sequenced using
120 Oxford Nanopore Technologies (ONT). The read counts of integrated DNA versus wildtype DNA
121 are then compared. The amount of integration is dose dependent. The high level of episomal
122 vector genomes (VGs) in the vector-treated samples prevents the ddPCR method from being
123 used.

124 **Figure 1: Integration of hPAH into human PAH locus**

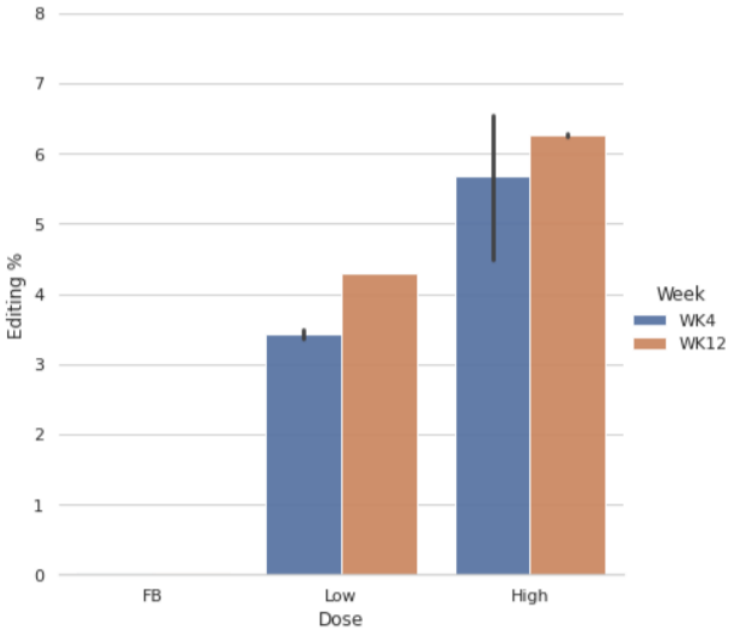

125

126 **Figure 1:** FRG mice were treated with formulation buffer (FB), 7E+13 VG/kg (Low), or 2E+14 VG/kg (High)
127 of hHA-LP1-hPAH. After either 4 (blue) or 12 weeks (brown), mice were sacrificed, and livers removed
128 for isolation of human hepatocytes and DNA analysis.

129

130 **Predicted Off-target integrations**

131 If rAAV vectors were to integrate at genomic sites other than their intended targets, it is most
132 likely that such off-target integrations would be directed toward homologous sequences.
133 During vector design, homology arms were chosen to have minimal sequence identity with the
134 rest of the genome. As a result, all sequences elsewhere in the genome are poor matches for
135 the hHA-LP1-hPAH homology arms. To test the most likely of the poor matches, predicted off-
136 target integration sites were selected based on two criteria, a minimum sequence length of 35
137 bp and a minimum sequence identity of 60% relative to any sequence in the homology arms.
138 Only six genomic regions could be identified that met both these criteria. The six identified
139 regions had 38-52 bp homology with 60-85% identity relative to the hHA-LP1-hPAH homology
140 arms. Because the sequence of both the homology arms and the predicted integration site is

141 known, it is straightforward to design primers that allow specific amplification for putative off-
142 target integration sites at 5 of these 6 regions (Supplemental Table 1).

143 To generate positive control DNAs for the potential integration sites, gBlock DNA was
144 synthesized that contained a sequence corresponding to what the putative integration sites
145 would have if the junctions were present in the genome. These were used to spike into control
146 human genomic DNA at molar ratios starting at 1:10 and serially diluting 10x down to 1:10,000.
147 Each spiked, positive-control integration site could be detected at all ratios when amplified with
148 the integration-specific primers. This established the limit of detection as 1 in 10,000. When
149 genomic DNA from the FRG mice treated with hHA-LP1-hPAH was tested, no signal at any of the
150 predicted off-target sites could be detected (Figure 2), indicating that the five tested sites were
151 not subject to off-target integration at rates above the Limit of Detection (LoD).

152 **Figure 2: Analysis of Predicted Off-Target Integration**

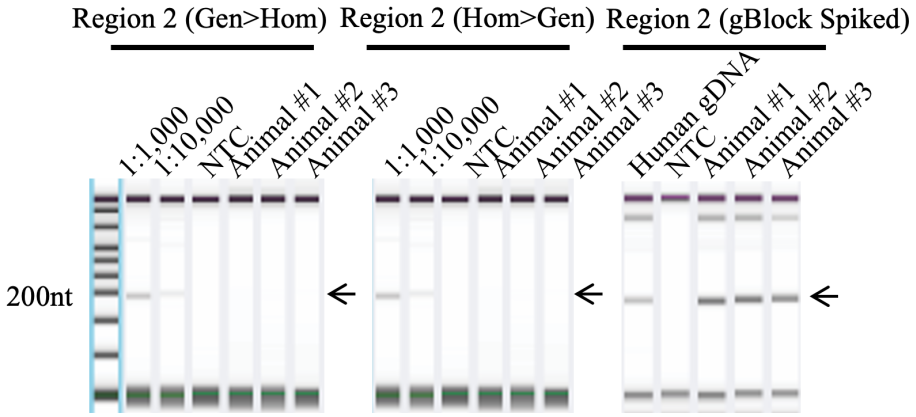

153

154 **Figure 2:** Human genomic DNA was amplified for five predicted off-target sites (Supplemental Table 1).
155 TapeStation profiles for Region 2 are shown. Positive control gBlock DNAs are shown for spikes of
156 1:1000 and 1:10,000 with PCRs from the genomic region (Gen) to the right of the potential integration
157 towards the homologous region (Hom) and from the homologous region to the genomic region to the
158 left side of the possible integration. Genomic DNA from three animals treated with vector is shown for
159 these amplifications and for a No Template Control (NTC). In the right panel, human genomic DNA and
160 DNA from the same three animals are amplified in the presence of the positive control gBlock DNA to
161 demonstrate that amplification would be possible if the off-target integration had occurred.

162

163 **Genome-wide Integration Assay (GWIA)**

164 *Amplification specificity*

165 Examination of predicted editing sites is the only measurement done when some editing
166 technologies are evaluated.[27] However, it is preferable to examine all potential integration sites
167 more broadly to characterize the editing/integration process fully. When scanning the entire
168 genome for any potential integration sites, selectivity can be achieved by using a specific primer

169 for the vector payload, but the same degree of selectivity is not possible for the unknown
170 genomic sequence adjacent to uncharacterized off-target integrations. Furthermore, the
171 payload-specific primers provide specificity relative to genomic DNA, but episomal DNA
172 contains the identical sequences as the integrated DNA so that primer provides no specificity
173 relative to the problematic contaminating episomes. These can be present at up to thousands
174 of fold excess relative to integrated DNA, creating a serious signal to noise issue. There are
175 many methods to select for or against specific sequences (such as affinity tags), but we have
176 not found these to be robust when used to select for or against AAV episomal DNA containing
177 ITRs. Two techniques were found to aid specificity in this situation, the use of splinter adaptors
178 attached to the genomic end of the DNA and use of chimeric Locked Nucleic Acid (LNA)
179 oligonucleotides to selectively block episomal amplification at episome-specific regions. Both
180 methods have been used previously during the characterization of other viral integrations.[28]

181 While the payload primer on one end of the amplified integration junction provides specificity
182 for that DNA end, the primer on the other end must be sequence-agnostic to allow the
183 detection of any region in the genome. This specificity limitation can be partially ameliorated
184 via the use of splinter adaptors.[28] Splinter adaptors are a pair of oligonucleotides that are
185 partially complementary to each other. They consist of a longer DNA with an extended 5' end
186 and a shorter DNA that is blocked at its 3' end to prevent extension even in the presence of the
187 longer sequence. These adaptors are ligated to the repaired ends of all free DNAs. Amplification
188 starting from the splinter end of the DNA can only be achieved if the 5' extension is initially
189 replicated from another priming site located nearby (schematic in Supplemental Figure 2).
190 Ideally, activating replication occurs only when the payload-specific primer is extended, but
191 other artifactual sources of copying could also happen and replicate the longer splinter adaptor,
192 making it available for artifactual priming. Nonetheless, the payload-primer specificity at the
193 vector DNA end is assisted by some degree of specificity at the genomic end of the amplicon
194 using splinter adaptors.

195 Another method for further improving specificity is using LNA oligonucleotides to block the
196 amplification of unwanted episomal DNA.[29] Because LNAs bind tightly to DNA, they can prevent
197 DNA amplification when 3' blocked and bound to specific sequences. In each of our rAAV
198 vectors, short sequences are located between the homology arms and the ITRs that are present
199 in the episomal DNA but not in the HR-integrated DNA. Binding LNAs to this region does not
200 affect amplification of HR-integrated DNA but significantly inhibits amplification of the episomal
201 DNA. LNAs of 20-24 nt were found to be specific and effective for this purpose.[29] Various other
202 methods to improve selectivity were tested, but the challenging nature of rAAV was found to
203 limit their usefulness for either positive or negative selection.

204 Using nested PCR with splinter primers and LNA blocking, the GWIA method (Figure 3) was
205 developed. DNA containing the codon-optimized vector payload (CO-hPAH) fused to human
206 genomic sequences irrespective of where those human genomic sequences are located is
207 amplified preferentially and independently of location, so it is possible to simultaneously detect

208 low levels of both on- and off-target integration. Unfortunately, like other integration assays,
209 GWIA is subject to artifacts so appropriate controls need to be included to avoid problem
210 sequences like telomeric DNA that may self-prime, mitochondrial DNA that is present at
211 thousands of copies per hepatocyte[30] and repeat sequences that may misprime off each other.
212 Additionally, unintegrated episomal VGs can significantly disrupt amplification due to their
213 appetite for vector-specific primers. The excess vector DNA also contributes to two primary
214 sources of artifactual signals that interfere with the detection of integration events. First, the
215 episomal DNA can ligate to fragmented genomic DNA during sample processing, generating a
216 false positive integration signal. Second, cells containing high levels of VGs can create a
217 multitude of concatemers and other recombinants in which VG DNA may be rearranged into
218 configurations that allow efficient amplification with one or two primers, increasing noise,
219 reducing primer availability, and making true positive signals hard to distinguish. The degree to
220 which these artifacts obscure the detection of true signals depends on the nature and
221 concentrations of VGs and must be evaluated in multiple conditions so that the effective
222 detection range of GWIA can be determined.

223 **Figure 3: GWIA Schematic**

224

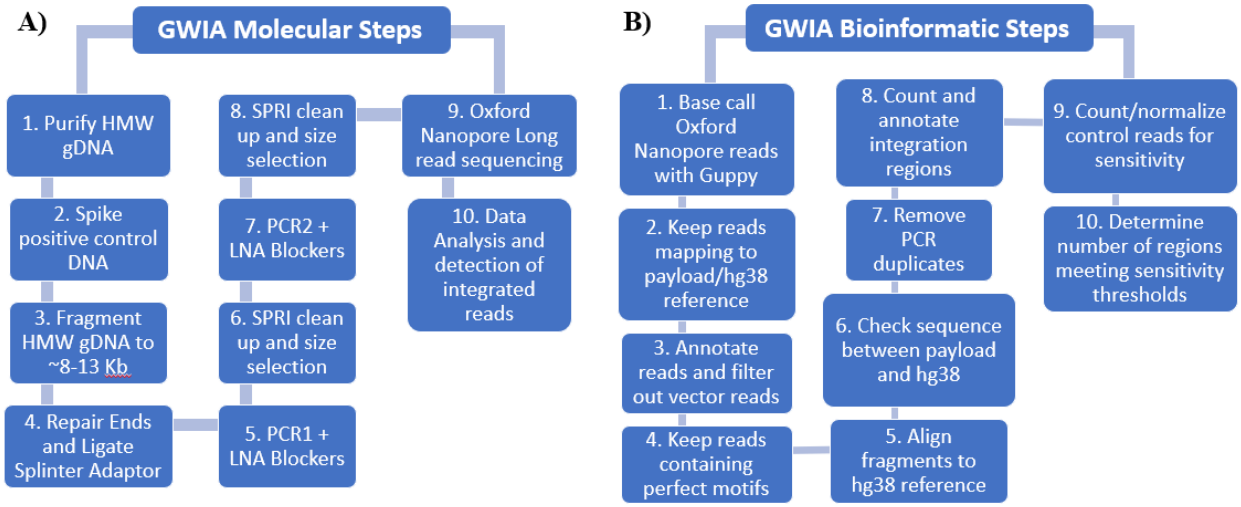

225

226 **Figure 3:** Schematic flows for laboratory and informatics steps in the GWIA methods are listed. A more
227 complete listing of details is provided in methods.

228

229 **Positive control DNAs**

230 On-target integration occurs at up to ~6%, but off-target integration, if it occurs at all, is much
231 less common, making it more challenging to detect. Thus, generating a positive control for
232 determining the LoD is imperative. There are multiple literature examples of purported viral
233 integration findings that were later challenged by others as being caused by artifacts rather
234 than real integrations,[15,31,32] and it would not be surprising to find additional examples with

235 AAV, especially with samples rich in vector episomes. Sample and library processing can
236 generate various artifacts that share some properties with integration events but are not
237 authentic integrations. To address this, we have developed two types of positive control DNAs
238 for assessing LoD: a series of plasmids containing pseudo-off-target integration junctions and a
239 cell line with an on-target integration that includes SNVs to distinguish it from authentic on-
240 target integrations. For the plasmid positive control off-target DNAs, 36 random fragments of
241 human genomic DNA were cloned adjacent to the right homology arm. These plasmids were
242 sequenced to identify the origin of their genomic DNA, and they were found to arise from
243 diverse genomic regions (Supplementary Table 2).

244 While the control plasmids allow us to query many different sequence contexts, independently
245 prepared, high quality plasmid DNA may behave differently than the longer genomic DNA. To
246 assess sensitivity and specificity using genomic DNA, a cell line was generated to provide an
247 additional positive control for on-target, genomically integrated vector. A plasmid containing
248 the payload region with variants to distinguish it from the standard gene therapy vector was co-
249 transfected with CRISPR-Cas9 molecules containing sgRNAs targeting two sites in the chr12
250 region at which integration was intended. In a fraction of the cells, CRISPR-Cas9 cleaves the
251 targeted locations which can then be repaired using the plasmid with the slightly variant
252 homology arms. Because this repair could occur via Non-Homologous End Joining (NHEJ) and
253 may not be HR-directed, this recombination may be different than what would occur with the
254 virus and errors might be introduced in or near the integration site. Other off-target, CRISPR-
255 dependent sites might also generate integration events.

256 After transfection of the plasmid and CRISPR-Cas9, cells were single-cell cloned and expanded.
257 The resulting individual clones were screened by PCR for the desired chr12 integration event.
258 Clones that appeared to contain the correct junction DNA by PCR were sequenced using Oxford
259 Nanopore. One cell line with an appropriate integration (A11) was found which also contained
260 normal genomic DNA in the same region, indicating the integration event had occurred in only a
261 single chr12 allele. In addition to this planned integration event, another complex event was
262 detected via GWIA that included a segment of chr17 and multiple vector payloads. Whole-
263 genome sequencing of A11 with PacBio was performed to characterize the integration pattern
264 better. In addition to the expected CRISPR-driven integration event on chr12, the second,
265 unexpected integration event included >2 kb from chr17 and multiple payloads and vector
266 cloning sites but only a small segment of ITR. The complexity and length of this integration
267 region prevented complete assembly. DNA prepared from this cell line has been used as a
268 positive control by spiking into assays of test genomic DNA at known amounts to evaluate the
269 sensitivity of the GWIA method for detecting integration.

270 To confirm the blocking ability of LNAs in this system, genomic DNA from A11 was amplified
271 using three primers. One primer is in the PAH payload sequence and is present in both the on-
272 and off-target integrated DNA. The other primers were designed to match adjacent genomic
273 DNA from the intended on-target site in chr12 and the observed off-target site in chr17. The

274 chr17 off-target site includes a vector sequence not present in the HR-like integration event on
275 chr 12 and the blocking LNAs target this vector sequence. When no LNAs are present, these
276 DNA fragments are amplified equally efficiently whether alone or together (Supplemental
277 Figure 3, lanes 1-3). When the vector-specific blocker is added (lanes 4-6), chr17 amplification is
278 blocked whether alone (lane 4) or in combination with the chr12 primer (lane 6), confirming
279 that LNA can specifically block vector sequence amplification.

280

281 **Limit of Detection (LoD)**

282 The 36 different plasmid control DNAs with artificial integration junctions were spiked into A11
283 genomic DNA at varying relative concentrations and subjected to GWIA to assess both on-
284 target integration provided by the A11 DNA and off-target integration provided by the 36
285 different plasmids. GWIA is described in detail in Materials and Methods with a schematic of
286 the laboratory and analysis workflow shown in Figure 3. Briefly, genomic DNA is spiked with
287 appropriate controls, sheared to ~8 kb, repaired, ligated to splinter adaptors, amplified with
288 one pair of payload/splinter primers in the presence of LNA blockers, size selected, amplified a
289 second time with a different, nested pair of payload/splinter primers in the presence of LNA
290 blockers, size selected, and sequenced using Oxford Nanopore flow cells. The resulting data is
291 then base-called, aligned to vector and hg38 references, and filtered based on multiple
292 sequence motifs.

293 When plasmids are spiked into A11 positive control genomic DNA and analyzed relative to on-
294 target reads from A11, the recovery of plasmid "integration" reads is consistent across all
295 sequence types (Figure 4). This shows that it is possible to detect off-target integration events
296 mimicked by the plasmids across a wide variety of sequence contexts when those integration
297 junctions are present. To further assess the assay's sensitivity for low levels of integration
298 junctions, varying concentrations of the different plasmids were spiked into genomic DNA over
299 a 1000-fold range starting at a 1% molar ratio relative to genomic DNA and going down to
300 0.001%. Detection over a 100-fold range was reasonably linear (Figure 5), but the lowest
301 concentration was not readily detectable in these conditions. Thus, when the DNAs are of good
302 quality and unencumbered by contaminating VGs, detection of integration junctions down to
303 0.01% can be readily achieved.

Figure 4: Read Frequency for Positive Control Plasmids using GWIA

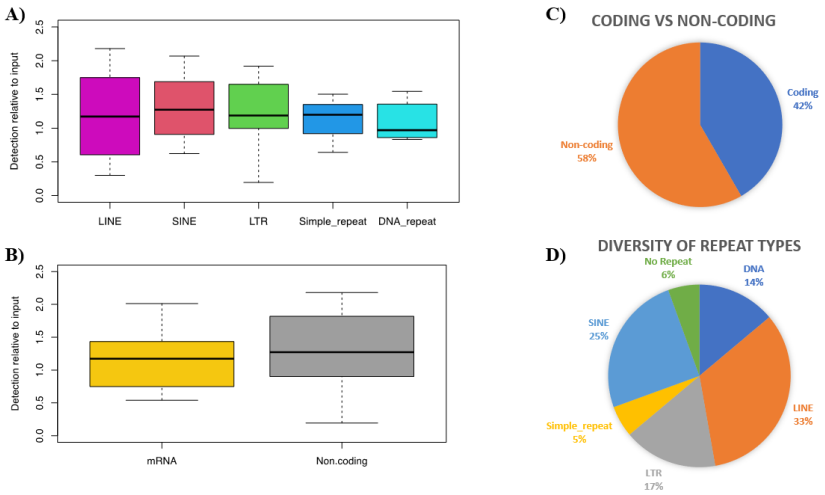

Figure 4: Sequences cloned adjacent to RHA were classified as their repeat content and whether they contained coding or non-coding sequence. Relative read counts for each junction were made and averaged by class.

Figure 5 Detection of Control Plasmid DNAs

A)

Dilution	Plasmid 1	Plasmid 2	Plasmid 3	Plasmid 4	On Target	Off Target	On Copies	Off Copies
1	hOT-5	hOT-6	hOT-7	hOT-13	1X	0.01X	200,000	2000
2	hOT-14	hOT-15	hOT-18	hOT-21	1X	0.001X	200,000	200
3	hOT-24	hOT-28	hOT-30	hOT-31	1X	0.0005X	200,000	100
4	hOT-36	hOT-37	hOT-40	hOT-12	1X	0.0001X	200,000	20
5	hOT-17	hOT-23	hOT-20	hOT35	1X	0.00001X	200,000	2

B)

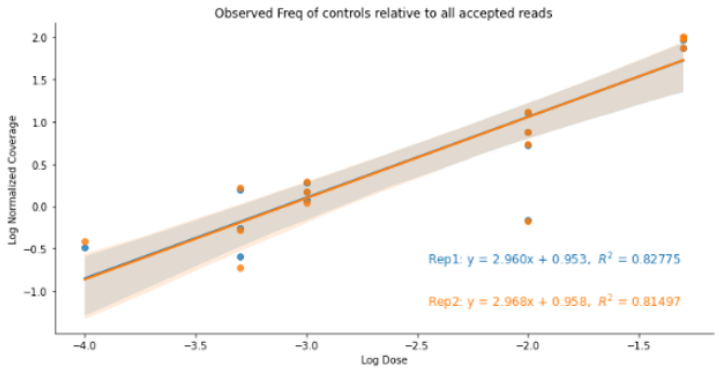

Figure 5: Twenty plasmids with RHA-genomic fusions were split into four groups and diluted as listed in A. Each mix was sequenced and reads were assigned to the different plasmids. The correlation of dilution and read count is shown (B).

315 **Limit of Blank (LoB) in the presence of VGs**

316 AAV capsids lysed via heat treatment release both plus and minus strand ssDNA and the
317 complementary strands rapidly anneal to generate dsDNA from the +/- ssDNAs. This dsDNA can
318 be spiked into reactions to assess VG-dependent artifacts. However, because the VG DNA was
319 never in cells after packaging, the spiked DNA does not contain any integrated or concatemeric
320 DNA like that potentially generated inside cells. Control genomic DNAs from either human or
321 mouse were spiked with varying concentrations of lysed vectors and A11 genomic DNA (Table
322 1) to mimic the composition of DNA in transduced cells with no non-control integrated DNAs
323 present. The lysed vectors were spiked before fragmentation, but their smaller starting size
324 relative to genomic DNA makes it likely they are minimally affected by the shearing.[33] In these
325 samples, the starting molar ratio of vector to human DNA ranges from 100:1 to 10,000:1.
326 Depending on the injected vector dose, the actual ratio in hepatocytes treated with high doses
327 of rAAV can be up to 1000:1. With the highest ratios of vector DNA, very little human DNA is
328 detected because most of the reads are episomal DNA that likely undergoes linear or inefficient
329 amplification. As the amount of lysed vector is decreased, the number of RHA reads increases
330 as well as the number of reads with both RHA and hg38 sequence. The amount of linearly
331 amplified vector decreases while the human DNA is amplified better. However, even with the
332 lowest amount of lysed vector, nearly 90% of reads contain neither RHA nor other human
333 sequences, showing the preponderance of artifactual vector sequences that are amplified
334 despite efforts to minimize their impact.

335 When A11 genomic DNA is also added along with the lysed vector, the number of total reads
336 drops substantially, but, depending on the amount of A11 added, the number of reads
337 corresponding to RHA and hg38 increases. The number of reads with CO-PAH, RHA, and hg38
338 sequences in the correct locations for integration is much higher with the A11 spike. However,
339 amplification of the A11 integration site is clearly non-linear as very few A11 reads are seen
340 with 1% A11 DNA added while more than 10x as many reads are seen with 2.5% and 5% A11
341 DNA. Some sequences also correspond to off-target sites, but almost all of them are singletons
342 that are not conserved across samples. Because no integrated DNA can be present, these must
343 all be false positives arising from artifactual processes. The presence of false positive
344 integration signals in DNA controls where no integration could have occurred highlights the
345 need to determine the LoB in different conditions. Furthermore, any suspected off-target
346 integration event should be confirmed in tested samples via PCR with custom designed primers.

347

348 **GWIA in Engrafted Human Hepatocytes**

349 The use of control plasmid and genomic DNAs to model the behavior of DNA from treated cells
350 could be incomplete because the rAAV DNA from capsids transduced into cells can undergo
351 complex rearrangements that are not readily mimicked by the control DNAs prepared in vitro.
352 To better understand the impact of in vivo VGs, A11 control genomic DNA was spiked into

genomic DNA isolated from human hepatocytes from engrafted FRG mice treated with varying amounts of vector for different times post-injection. These samples contain the full range of DNA species including episomal vectors, concatemers, and other vector rearrangements that may arise over time in cells. The various DNAs may behave unexpectedly during library preparation, leading to artifacts including non-specific ligation to other DNA fragments and primer-independent (via ITRs) or single primer amplifications. As shown in Figure 6, increasing concentrations of A11 control DNA spiked into the samples from mice dosed at 7E+13/kg yields a reasonably linear response. The episomal VG load in these cells was determined using qPCR measurements. This assay does not distinguish between monomeric episomes and more complex concatemeric structures. The low-dose samples average 47 CO-PAH copies /allele. At the higher dose, 2E+14/kg (average of 79 CO-PAH copies/allele), the response is no longer linear and flattens above 3% A11 DNA. Thus, it is possible to detect the integration junctions but not accurately estimate their frequency using GWIA in high VG conditions.

Figure 6: Limit of Detection in FRG Mice with A11 Spike

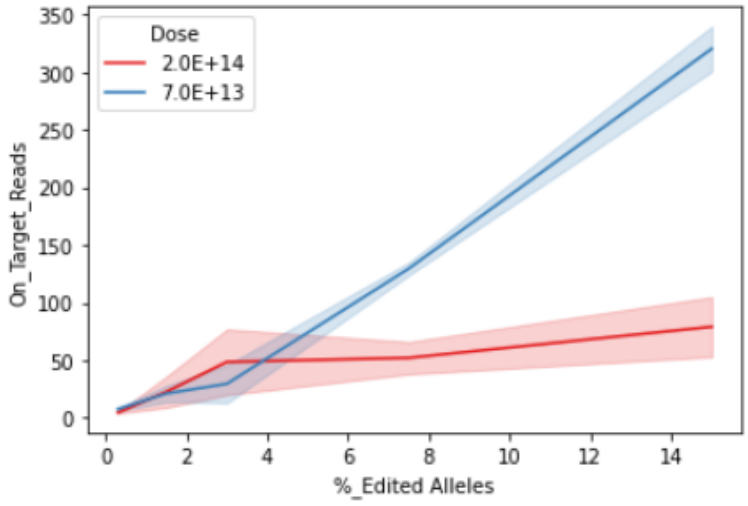

Figure 6: On-target integration reads from A11 were counted for all FRG mice treated with hHA-LP1-hPAH. The number of A11 reads as a function of spiked DNA fraction is shown for the low- and high-dose animals.

It is also instructive to examine reads that are filtered out during informatic analyses. By far, the two filters that eliminate most of the reads require that the resulting sequences have regions that map to the RHA and a separate region that maps elsewhere in hg38. This eliminates over 99% of reads in all cases and highlights the rarity of events sought. Other filters that have a lower impact include those eliminating reads with vector sequence beyond RHA and those where the RHA and other hg38 sequences are separated by more than 30 bp. When the intervening sequence is longer than 3 bp, it is usually random and cannot be aligned. Authentic junction sites tend to have 0-3 bp between the RHA and hg38 regions with that variable segment generally caused by sequencing errors. PCR duplicates, which are assigned based on

380 the positions of the RHA and gDNA breakpoints, are also removed, but these are infrequent
381 given the low number of junctions found.

382

383 **Off-target integration in engrafted hepatocytes**

384 Based on the findings that 2.5% A11 DNA spiked into genomic DNA from engrafted human
385 hepatocytes would provide the best sensitivity in the treatment range we performed, we
386 examined genomic DNA purified from human hepatocytes from mice four or twelve weeks
387 after injection. FB-treated mice had no episomal VGs and thus could not generate concatemers
388 that could amplify and compete with the integration signal. FB-treated mice had ~100x more
389 positive control reads than hHA-LP1-hPAH treated mice. Additionally, the low-dose hHA-LP1-
390 hPAH treated mice had more positive control reads than the high-dose hHA-LP1-hPAH treated
391 mice due to lower interfering VG levels. All replicate samples had on-target reads that were
392 within 2x of each other. Only the on-target integration site on chr12 generated more reads than
393 the positive control cell line genomic DNA used to establish LoD. No genomic regions had reads
394 higher than the 0.5% LoD based on the number of reads from the spiked genomic DNA. The
395 location of integration junction reads is shown in Figure 7. While the intended site is easily
396 observed, all other reads were sporadic and likely due to library artifacts. If any significant off-
397 target sites had been identified, PCR primers would have been designed to determine whether
398 the purported events were real.

399 The diversity of sequence ends is shown in a representative Integrative Genomics Viewer (IGV)
400 file displaying ONT sequencing reads from one low-dose hHA-LP1-hPAH sample (Figure 7). Each
401 single molecule read contained sequence starting with the CO-hPCR primer located on the left
402 end and going through the RHA region into adjacent genomic DNA (up to thousands of bases
403 depending on the position of the shearing site) and ending with the adaptor ligated to the end
404 of the randomly fragmented genomic DNA. The range in length distributions observed on the
405 right end of the reads is caused by the reverse primer binding to the adaptor ligated to the
406 randomly sheared ends of different molecules.

407 **Figure 7: GWIA in Transduced Engrafted Human Hepatocytes**

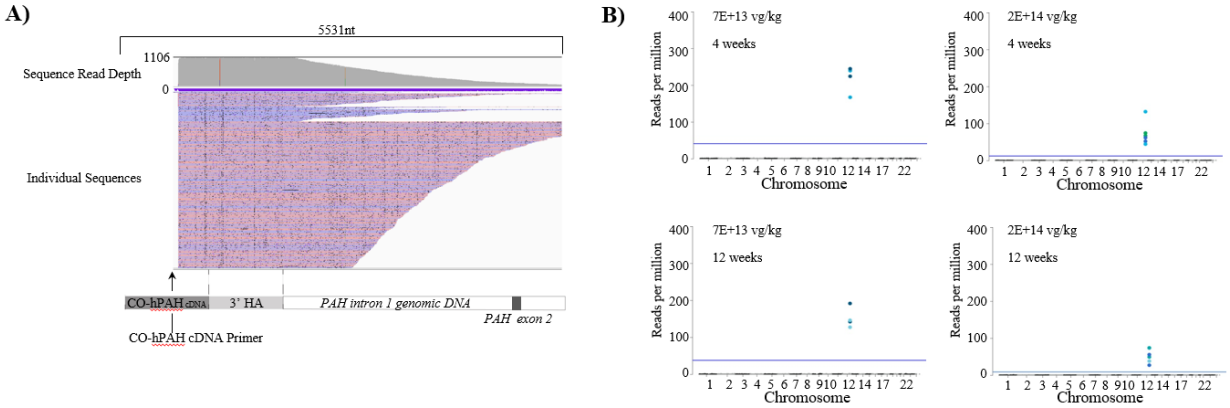

408

409 **Figure 7:** A) IGV view of reads mapping to the on-target integration site on chr12. Each line corresponds
410 to an individual, non-duplicated read. Blue and pink colors indicate the orientation (+/-) of reads. The
411 map of the integration region is shown below the reads. B) The on- and off-target reads for each animal
412 are shown in a Manhattan plot. The LoD is shown as a horizontal line. Only the on-target reads are
413 visible because off-target reads are too infrequent.

414

415 Many artifacts arise in an unknown manner and could come from events that occur in the cell
416 or during subsequent library preparation, ligations, and amplifications. Three reads from the
417 FRG mouse samples are interesting because they are fusions of lambda DNA with human DNA.
418 If lambda had been injected along with rAAV, these might be ascribed to lambda integration
419 into human genomic DNA. However, lambda is only present at the last stage of library
420 preparation where it is added as an ONT sequencing control and is found well below the LoD.
421 These findings highlight the potential for ligation or PCR-induced artifacts arising during sample
422 processing.

423

424 **[Discussion]**

425 AAVs have shown durable expression in the liver using AAV gene therapy for hemophilia, with
426 human data out to 7 years[34] and canine data out to 10 years.[35] More recently, AAV delivery of
427 a functional *PAH* gene has been shown to restore the normal biochemical pathway in a mouse
428 model of PKU and is currently in clinical trials for adults with classical PKU.[24] The preclinical
429 studies demonstrated durable expression of human PAH in PAH^{enu2} mice and normalization of
430 Phe out to a year post-dose (end of study). This approach used AAV-based gene therapy to
431 deliver and express the gene extra-chromosomally in episomes. As the transduced cells divide,
432 dilution of the episomes can occur given that the episomes do not replicate with cell division.
433 While hepatocytes in the adult liver divide over time, this process is relatively slow compared to
434 a growing liver during childhood development. For a disease like PKU that is diagnosed shortly

435 after birth, a gene editing-based therapy with durability through liver growth and hepatocyte
436 turnover may benefit adults as well as younger individuals.

437 Several approaches aiming to correct the underlying mutation in PKU have been reported.
438 Villiger et al[36] showed that using two AAV vectors, delivery of a Crispr-Cas9-base editor
439 targeting the PAH^{enu2} mutation could correct the mutation in the liver resulting in a reduction of
440 serum Phe to normal levels. Richards et al[37] showed that using a dual vector approach
441 delivering two doses (at 1 and 5 weeks of age) of a Crispr-Cas9 nuclease specific to exon 7
442 downstream of the PAH^{enu2} mutation and a 2.7 kb repair template encoding the corrected
443 variant resulted in serum Phe lowering that was sustained for 65 weeks. This approach relied on
444 the homology-directed repair (HDR) mechanism to correct the PAH^{enu2} mutation. In this case,
445 the percentage of HDR-modified alleles averaged 13%, with 7% showing functional correction
446 at the cDNA level, and resulted in Phe reduction, but not to normal levels. More recently, Bock
447 et al[38] showed that using AAV8 and AdV to deliver a size-reduced *SpCas9* prime editor could
448 achieve 11% editing in the PKU model, resulting in serum Phe concentrations below the
449 therapeutic threshold of 360 μM.

450 While these approaches are promising, they target a specific mutation in the *PAH* gene and are
451 not directly applicable to the thousands of other *PAH* mutations. Furthermore, like many other
452 CRISPR-based approaches, potential off-target events were not examined in a whole-genome
453 manner. Others have easily identified large structural effects induced by CRISPR.[39] However,
454 potential single base changes cannot be readily evaluated across the whole genome because
455 the background level of single base changes that occur with every round of replication can
456 obscure the signal from such potentially deleterious modifications.[40] Targeted assessment of
457 the most likely hot spots for editing can be carried out, but most of the genome remains
458 unevaluated for mutations. HR-driven AAV integration events are easier to detect and
459 distinguish from any background activity because of their larger size and unique sequence
460 characteristics.

461 Two particularly important artifacts must be addressed when attempting to identify real AAV or
462 other viral integration events: 1) Processing-dependent ligation of AAV fragments to other
463 DNAs that may appear to be fusion events but are simply in vitro ligation artifacts; and 2) use of
464 short read sequencing technologies to assemble long molecules that may not actually be
465 present when examined as long reads. Indeed, a study comparing NGS methods that included
466 controls showed that ligation was a significant driver of false positives in control samples.[19] Use
467 of transposase instead of ligase reduced artifacts.

468 Because of the high background of AAV genomes and their propensity for generating
469 concatemers, amplification of minor components can lead to unexpected fragments whose
470 source could be attributed to integration rather than be correctly identified as artifacts. Some
471 artifacts, like PCR mispriming, can be readily detected by appropriately examining the
472 sequenced DNA[23] while others can be more challenging. Because our nested PCR primers do
473 not extend to the end of the splinter adaptors, we can eliminate mispriming as a significant
474 cause of artifacts in our system because those sequences are not present in our products. We
475 have included relevant positive controls and long-read sequencing in our methods to ensure
476 that we can distinguish real integration events from artifacts at our stated sensitivity.

477 Awareness of artifacts in the study of viral integration is recognized as an issue in the literature.
478 Kaeppel *et al.* (2013)[41] reported a significant number of mitochondrial-AAV integrations, but
479 this result was challenged by Cogne et al (2014),[15] who used an alternative approach to
480 minimize artifacts. The response to this challenge cited new experiments with controls
481 intended to address the issues raised, but the new controls either contained no AAV DNAs or
482 no primers that would allow their amplification. Thus, the original issues raised remain relevant
483 and it is possible that the insertion events identified could be simply processing artifacts and
484 not actual integration events. Similar integration artifacts have been observed and challenged
485 when looking at other putative viral "integrations".[31,32] Any potential off-target integration
486 events need to be confirmed using an orthogonal method, like directed PCR, before citing their
487 occurrence.

488 While it would be desirable to achieve much greater sensitivity when examining off-target
489 integration, it is not generally possible to do so with the limitations of sample availability and
490 the sequence similarity with episomes. While efforts to improve sensitivity will continue, it is
491 worth noting the safety record of rAAV across systems. After 10 years post-administration of
492 AAV8 or AAV9 vectors expressing canine factor VIII, none of the dogs showed evidence of
493 tumors, altered liver function, or any liver pathology features that could be attributed to
494 treatment with AAV.[42] George et al. published a follow-up study in humans treated with AAV
495 expressing Factor 9 and also found no evidence of liver toxicity or other major safety concerns
496 out to 15 years post-dose.[35] An earlier study concluded the same lack of hepatic genotoxicity in
497 nonhuman primates and humans.[43]

498 A hallmark of AAV-mediated HR is the precision of integration and avoidance of unwanted
499 mutations. HR is the preferred DNA repair pathway for the gain-of-function insertion of DNA
500 given the precision and lack of insertions/deletions that could disrupt expression as seen with
501 nucleases and base editors. Previous work using short-read NGS showed that AAVHSC15-
502 mediated integration did not introduce indels or ITR sequences at the target integration site.[22]
503 The use of long-read sequencing is critical in these studies to ensure that genomic DNA is being
504 analyzed and not the much higher copy number episomal DNA. Confirming the desired
505 integration is a crucial safety assessment for integrating vectors. When evaluating across the
506 genome using long-read NGS, the only site of DNA integration detected above the LoD was at
507 the desired human *PAH* locus.

508

509 **[Methods]**

510 **Animal Procedures for Mice.**

511 Housing, breeding, and all procedures performed on PAH^{enu2} mice were in accordance with the
512 Institutional Animal Care and Use Committee (IACUC) at Homology Medicines, Inc.

513 The FRG mice were housed in an IACUC accredited facility. General animal care and housing
514 procedures are described in Guide for the Care and Use of Laboratory Animals, National
515 Research Council, 2011, Yecuris™ IACUC Policy, and Yecuris™ General Mouse Handling Care and

516 Euthanasia. Cage changes occurred every 2 weeks and the testing facility was sanitized weekly.
517 Animals were provided irradiated mouse chow with a low Tyr content (0.53%, PicoLab® High
518 Energy Mouse Diet, 5LJ5 chow) and drinking water ad libitum. Animals were administered the
519 prophylactic antibiotic sulfamethoxazole and trimethoprim (SMX/TMP, 80 mg/mL/16mg/mL)
520 every other week in their drinking water. They were administered 2-(2-Nitro-4-
521 trifuoromethylbenzoyl)-1, 3-cyclohexanedione (Nitisinone, NTBC) for 3 days once every month.

522 **$Fah^{-/-}/Rag2^{-/-}/Il2rg^{-/-}$ (FRG®) Humanized-Liver Xenograft Mouse Model.**

523 The $Fah^{-/-}/Rag2^{-/-}/Il2rg^{-/-}$ (FRG®) mouse model has been characterized by Azuma et al.[26] In brief,
524 engrafted human hepatocytes integrate completely into the structure of the recipient mouse
525 liver and occupy greater than 80% of the parenchyma without disturbing the recipient liver
526 organization. Human hepatocytes can be distinguished morphologically from mouse
527 hepatocytes. From a functional perspective, engrafted human hepatocytes retain the functional
528 properties of mature, differentiated hepatocytes as demonstrated by the expression of mature
529 hepatocyte-specific genes and albumin secretion. Typically, 75% of the transplanted mice
530 achieve and maintain high levels of long-term engraftment, demonstrated by histology, DNA
531 analysis and enzyme assays. The majority of the mice that survive the procedure have high
532 levels of engraftment based on circulating human albumin levels and post-mortem histology.[44]

533 To generate humanized livers in FRG mice, human primary hepatocytes are implanted
534 concurrently with the withdrawal of 2-(2-Nitro-4- trifuoromethylbenzoyl)-1, 3-
535 cyclohexanedione (Nitisinone, (NTBC) that is required for survival by mouse hepatocytes in this
536 strain. Since the human hepatocytes have an intact fumarylacetoacetate hydrolase (FAH) gene,
537 only mouse hepatocytes are affected by the loss of NTBC, resulting in the gradual repopulation
538 of the mouse liver compartment with human hepatocytes.[26]

539 FRG mice achieve high levels of repopulation 5-6 months post-transplant and are typically used
540 within 6-8 weeks to avoid natural loss of engraftment or tumor development as they age.
541 Compared to wild-type mice, the FRG mouse model lacks B-cells, T-cells and NK-cells due to the
542 absence of the IL2rg and Rag2 genes. In addition, the remaining mouse hepatocytes do not
543 metabolize Tyr due to the lack of the *Fahah* gene. Despite these changes, this mouse model has
544 proven valuable in many research areas including infectious diseases, NASH, gene therapy,
545 metabolism and toxicology.[45-48]

546 The in-life and hepatocyte isolation portion of this study was conducted by Yecuris (Tualatin,
547 Oregon) who generated this model and have specialized technical expertise in handling this
548 mouse. Due to the complexity of the generation and handling of this model, the number of FRG
549 mice that can be utilized in a single experiment is limited.

550 **Injections:** 4- and 10-week-old PAH^{enu2} mice were weighed prior to injection, and a single I.V.
551 injection of the test article was administered retro-orbitally for all studies. Mice were
552 anesthetized using isoflurane for the injection. Proparacaine was applied to the eye before

553 injection. The needle was inserted into the retro-orbital sinus via the medial canthus and the
554 test article was injected slowly into the sinus. All doses were administered at 10 mL/kg.

555 FRG mice were removed from NTBC for ≥ 25 days and SMX/TMP for ≥ 3 days before dosing to
556 reduce the number of mouse hepatocytes. Mice were weighed before dosing and a single I.V.
557 injection of the test article was administered retro-orbitally using an insulin syringe (VWR,
558 Radnor, PA). One day post-dosing, the mice were put on NTBC and continued with the standard
559 NTBC water cycle for the duration of the study.

560 **Design and construction of AAV vectors**

561 The same AAV backbone plasmid, which included 5' and 3' AAV ITRs and flanking *PAH*-targeted
562 integration sequences, was used for all vectors. These vectors include a CO-hPAH DNA flanked
563 by locus-specific arms identical to human genomic sequences. The human 5' homology arm
564 aligns to human genome build hg38, chr12: 102916857-102917816 and the 3' homology arm
565 aligns to hg38 chr12: 102915806-102916716. The homology arms were selected to be unique in
566 the genome with no sequences of 40 nt or longer having homology to other locations. A late
567 SV40 polyadenylation sequence was included as a transcription termination sequence.
568 Promoter-containing vectors include the liver-specific promoter LP-1 as previously described,[49]
569 positioned between the 5' homology arm and the CO-hPAH DNA. The LP-1 promoter,
570 polyadenylation cassette and CO-hPAH DNAs were synthesized as gBlocks by IDT. The ITR
571 containing plasmid backbone, the CO-hPAH DNA, homology arms and regulatory sequences
572 were assembled by standard restriction digestion and ligation techniques.

573 **Test articles**

574 All vectors used were manufactured at Homology Medicines via a transient transfection process
575 using a HEK293 cell line. The vectors were packaged in AAVHSC15 capsid and are comprised of
576 an expression cassette as described above with or without the LP-1 liver-specific promoter,
577 human homology arms, and AAV2 ITRs on both ends of the construct. Vectors were diluted in a
578 pH-neutral buffer for I.V. administration. Vectors were tested for endotoxin (<10 EU/mL) and
579 titered by Droplet Digital™ polymerase chain reaction (ddPCR) using primers targeting the CO-
580 hPAH DNA. Vectors were analyzed for VP1, 2, and 3 ratios by silver- and Coomassie Blue-
581 stained SDS-PAGE and capsid titer by ELISA.

582

583 **Vector genome copy number by qPCR**

584 A real-time quantitative polymerase chain reaction (qPCR) method was used to quantify vector
585 genomes in mouse liver samples or isolated hepatocytes from FRG mice. Samples containing
586 gDNA and control plasmids were prepared for analysis on the ThermoFisher QuantStudio™ Flex
587 Real-Time PCR System, which utilizes TaqMan technology. The assay's linear range was 50 to
588 10E+8 copies per reaction with an LLOQ of 50 copies of vector per 1 µg of gDNA. Samples were
589 quantified against linearized plasmid. Real-time PCRs were performed on 96-well plates, and

590 each plate was run with a standard curve with no template control and study samples. The
591 standard curve was run with the plasmid in 3 replicates for the standard points at 1E+9, 1E+8,
592 1E+7, 1E+6, 1E+5, 1E+4, 1E+3, 1E+2, 10 and 1 copy per reaction. Vector-specific sequences were
593 amplified by real-time TaqMan PCR using the primers and probes for CO-hPAH (extended
594 methods). The PAH probe consists of the FAM™ fluorescence reporter dye at the 5' end of the
595 probe, the internal ZEN™ quencher (between the 9th and 10th nucleotides), and the Iowa
596 Black® fluorescent quencher at the 3' end of the probe.

597 **Analysis of on-target integration frequency by Oxford Nanopore sequencing**

598 On-target integration frequency was determined using a primer competition assay (3-primer).
599 The relative frequency of integration and non-integration sequences were tallied by long-read
600 Oxford Nanopore sequencing. The raw integration frequency was calculated as the percentage
601 of integrated reads divided by the sum of integrated and non-integrated sequences. The raw
602 frequency was corrected for a length-dependent PCR efficiency adjustment using
603 independently amplified DNAs and reduced by an additional factor caused by the amplification
604 of concatemeric sequences that interfered with the amplification of non-integrated sequences..

605 Each reaction included 100 ng of input genomic DNA. The frequency of integration by PCR was
606 normalized to a PCR efficiency curve. DNAs representing wild-type and integrated DNA were
607 mixed in known ratios. These templates were diluted and assayed by the PCR reaction as
608 described.

609 Purified WT and edited control templates were quantified with the Qubit 1X dsDNA HS assay
610 kit. The linear detection range of this assay kit is 0.1 ng/µL to 100 ng/µL. A stock control dilution
611 was made for WT and edited control templates in water, 1 ng/µL in 100 µL volume.

612 A concentration of 0.1 pg/µL was used as a working dilution for testing amplicon efficiency. 0.1
613 pg/µL contains ~70,000 copies of control template molecules. The amplicon efficiency test was
614 set up with 50% WT and 50% edited control templates with 0.1 pg total (0.05 pg WT and 0.05
615 pg Edited), so that the molecular number for the WT template is ~35,000 copies.

616 The resulting amplicons were prepared for Oxford Nanopore sequencing in accordance with the
617 manufacturer's instructions:

618 "Genomic DNA by Ligation (SQK-LSK109)" used for single-plexing:
619 https://community.nanoporetech.com/attachments/3041/download

620 "Native barcoding genomic DNA (with EXP-NBD104, EXP-NBD114, and SQK-LSK109)" used for
621 multiplexing with up to 24 barcodes:
622 https://community.nanoporetech.com/attachments/3186/download

623 Each amplicon to be sequenced was cleaned using AMPureXP beads and samples were
624 quantified using a Qubit 1X dsDNA HS kit. 200 fmol of input DNA was end-repaired. Each library
625 was purified by AMPureXP magnetic bead cleanup per the manufacturer's instructions. Up to

626 200 fmol of DNA was ligated to Nanopore barcoded adapter mix II and T4 DNA ligase followed
627 by AMPure bead cleanup and quantified by Qubit. DNA was prepared for final loading with 37.5
628 µL of sequencing buffer 25.5 µL of loading buffer and 12 µL of DNA library per flow cell. Each
629 library was loaded into the SpotON sample port and sequencing was initiated per the
630 manufacturer's instructions.

631 Analysis:

632 The resulting Fast5 files were base-called using Guppy basecaller. Only reads of the appropriate
633 amplicon size range between 1,100nt and 1,400nt were included. Reads which have plasmid or
634 vector sequences such as ITR were removed. All remaining reads were competitively aligned to
635 a WT and integrated genome reference sequence using the Minimap aligner. The raw read
636 frequency of wild-type and integrated sequences were tallied. Calculated "raw observed
637 integration %" = reads mapped to edited reference / (reads mapped to Edited reference + reads
638 mapped to WT reference). The standard curve of (0%, 0.5%, 1%, 2%, 5%, and 10%) was used to
639 generate linear regression formula for normalizing the raw observed % integration levels.

640

641 **Predicted Off Target**

642 Each homology arm was broken into 80bp windows, sliding 10bp per window, for a total of 171
643 windows. Each 80bp window was queried against the human genome (Database: RefSeq
644 Genome Database (refseq_genomes) Organism: Homo sapian (Taxid:9606)) with BLAST ((Expect
645 threshold: 10, Word Size: 16, Match/Mismatch Scores: 1,-2, Gap Costs: Linear) to identify
646 genome regions with >35bp match and >60% identity. From this analysis, 16 regions were
647 chosen as primary hits. Primary hits were then queried again with BLAT (UCSC Genome
648 Browser) to confirm the location and characterize the alignment. This narrowed the final list to
649 6 regions (supplemental table 1). One of the identified regions locates in a highly repetitive
650 genome locus. We dropped this region out of the analysis because we couldn't develop a
651 reliable PCR based assay (region 3).

652 Off-target analysis was carried out with 10 ng of genomic DNA from three transduced Yucaris human
653 hepatocyte samples. The amount of DNA available was limited so more could not be used. Each sample
654 was amplified for 35 rounds with primers specific to the predicted inward and outward integrations for
655 each identified region. Analysis of PCR products was done on a TapeStation to quantitate the anticipated
656 bands. For each region, the relevant synthetic DNA positive control was spiked into the human DNA
657 sample at two concentrations (1:1000 and 1:10,000) to ensure that the off-target band could have been
658 detected if present.

659

660

661

662 **Genome-wide integration assay (GWIA) by long-read Oxford Nanopore NGS**

663 GWIA experimental steps are summarized in Figure 3. gDNA from a positive control cell line
664 containing the PAH edited allele with added SNPs was spiked into all samples at a 2.5% molar
665 ratio. 500-1000 µg of total gDNA including spiked gDNA were randomly fragmented to ~8-
666 10kbp using COVARIS g-TUBES. Fragmented gDNA was end-repaired and A-tailed using the
667 NEBNext Ultra II End Repair/dA-Tailing Module, and ligated to splinter adapter
668 (GCCGAACATGAGCTATACGACTTAAACTTCCGCATGGCGTCTCCGCTTAAGGGACT; 5'Phos-
669 GTCCCTTAAGCGGAG-3'AmMO) with NEBNext Ultra II Ligation Module .[28] Ligated gDNA was first
670 amplified with a payload-specific, biotinylated forward primer (5'-
671 AAGACCGCCATCCAGAACTACA-3') and an outer splinter reverse primer (5'-ACTTAAACTTCCGCA
672 TGGCGT-3'). LNA blockers (/5AmMC6/CTGCA+G+G+T+C+T+A+G+ATACGTAG/3AmMO/;
673 /5AmMC6T/+AGATA+CGTA+GATA+AGTA+GCAT+GGC+G/3AmMO/;
674 /5AmMC6T/+AGATA+CGTA+GATA+AGTA+GCAT+GGC+G/3AmMO/;
675 /5AmMC6T/+AACCC+CTAG+TGAT+GGAG+TTGG+C/3AmMO/;
676 /5AmMC6T/+GGCGT+CGGG+CGAC+CTTT+GG+T/3AmMO/) against non-payload VG sequences
677 were used in PCR amplifications to limit episomal VG amplification. Biotinylated PCR1 products
678 were size selected with 0.5X SPRI beads (SPRIselect) twice (to remove unwanted <500bp
679 amplicons) and enriched by capture with streptavidin beads. Captured PCR1 products diluted at
680 1:100 were amplified again (nested PCR2) with the inner splinter primer (5'-
681 CTTAAACTTCCGCATGGC GTC TC-3') and an internal payload primer (5'-
682 AGAGGATCGAGGTGCTGGATAA-3'). Finally, PCR2 products were size selected with 0.5X SPRI
683 beads twice, and used to generate Oxford Nanopore libraries. Long-range sequencing was used
684 to provide sufficient sequence coverage to confirm the payload CO-hPAH DNA, the complete
685 homology arm, and adjacent genomic sequence. Sequencing data were analyzed with in-house
686 developed computational methods tuned to filter out VGs and artifactual reads. The positive
687 control cell line DNA spiked at 2.5% was used to estimate a lower limit of detection.

688 Analysis:

689 After sequencing, reads were base-called with Guppy and quality filtered with Filtlong.
690 Additional filtering was based on removal of the control lambda reads and any read that did not
691 contain the vector payload or DNA matching human genome sequences. Sequences were
692 annotated for components corresponding to vector. Reads with components that should only
693 be present in the vector were eliminated. Reads supporting the possibility of being integration
694 events were then filtered to eliminate sequences that did not meet criteria indicating they
695 arose from legitimate integration events. Such reads must include all or some of the RHA as
696 well as >200 nt following the 3' end of the RHA. This non-RHA region is then aligned to hg38
697 and those with MAPQ<40 or length <100 nt are discarded. Reads with more than 30 nt
698 separating RHA from hg38 are also discarded. PCR duplicates are collapsed to single reads.
699 Control reads were identified and counted to determine positive integration read cut offs.

700 Results from replicates were compared and only those appearing in both replicates were
701 considered real with the others discarded as technical artifacts.

702 Data Availability:

703 All fastq files used in this study have been uploaded to SRA under the accession PRJNA1001866.

704 **References**

705 1. Gao, G., Vandenberghe, L.H., Alvira, M.R., Lu, Y., Calcedo, R., Zhou, X., and Wilson,
706 J.M. (2004). Clades of Adeno-associated viruses are widely disseminated in human
707 tissues. J Virol *78*, 6381-6388. 10.1128/JVI.78.12.6381-6388.2004.
708 2. Gao, G., Alvira, M.R., Somanathan, S., Lu, Y., Vandenberghe, L.H., Rux, J.J., Calcedo,
709 R., Sanmiguel, J., Abbas, Z., and Wilson, J.M. (2003). Adeno-associated viruses undergo
710 substantial evolution in primates during natural infections. Proc Natl Acad Sci U S A
711 *100*, 6081-6086. 10.1073/pnas.0937739100.
712 3. Samulski, R.J., Zhu, X., Xiao, X., Brook, J.D., Housman, D.E., Epstein, N., and Hunter,
713 L.A. (1991). Targeted integration of adeno-associated virus (AAV) into human
714 chromosome 19. EMBO J *10*, 3941-3950.
715 4. Kotin, R.M., Siniscalco, M., Samulski, R.J., Zhu, X.D., Hunter, L., Laughlin, C.A.,
716 McLaughlin, S., Muzyczka, N., Rocchi, M., and Berns, K.I. (1990). Site-specific
717 integration by adeno-associated virus. Proc Natl Acad Sci U S A *87*, 2211-2215.
718 10.1073/pnas.87.6.2211.
719 5. Kotin, R.M., Linden, R.M., and Berns, K.I. (1992). Characterization of a preferred site on
720 human chromosome 19q for integration of adeno-associated virus DNA by non-
721 homologous recombination. EMBO J *11*, 5071-5078.
722 6. Barzel, A., Paulk, N.K., Shi, Y., Huang, Y., Chu, K., Zhang, F., Valdmanis, P.N.,
723 Spector, L.P., Porteus, M.H., Gaensler, K.M., and Kay, M.A. (2015). Promoterless gene
724 targeting without nucleases ameliorates haemophilia B in mice. Nature *517*, 360-364.
725 10.1038/nature13864.
726 7. Laoharawee, K., DeKelver, R.C., Podetz-Pedersen, K.M., Rohde, M., Sproul, S., Nguyen,
727 H.O., Nguyen, T., St Martin, S.J., Ou, L., Tom, S., et al. (2018). Dose-Dependent
728 Prevention of Metabolic and Neurologic Disease in Murine MPS II by ZFN-Mediated In
729 Vivo Genome Editing. Mol Ther *26*, 1127-1136. 10.1016/j.ymthe.2018.03.002.
730 8. Porro, F., Bortolussi, G., Barzel, A., De Caneva, A., Iaconcig, A., Vodret, S., Zentilin, L.,
731 Kay, M.A., and Muro, A.F. (2017). Promoterless gene targeting without nucleases
732 rescues lethality of a Crigler-Najjar syndrome mouse model. EMBO Mol Med *9*, 1346-
733 1355. 10.15252/emmm.201707601.
734 9. Miao, C.H., Snyder, R.O., Schowalter, D.B., Patijn, G.A., Donahue, B., Winther, B., and
735 Kay, M.A. (1998). The kinetics of rAAV integration in the liver. Nat Genet *19*, 13-15.
736 10.1038/ng0598-13.
737 10. Miller, D.G., Petek, L.M., and Russell, D.W. (2004). Adeno-associated virus vectors
738 integrate at chromosome breakage sites. Nat Genet *36*, 767-773. 10.1038/ng1380.
739 11. Drew, H.R., Lockett, L.J., and Both, G.W. (2007). Increased complexity of wild-type
740 adeno-associated virus-chromosomal junctions as determined by analysis of unselected
741 cellular genomes. J Gen Virol *88*, 1722-1732. 10.1099/vir.0.82880-0.
742 12. Schmidt, M., Schwarzwaelder, K., Bartholomae, C., Zaoui, K., Ball, C., Pilz, I., Braun,
743 S., Glimm, H., and von Kalle, C. (2007). High-resolution insertion-site analysis by linear
744 amplification-mediated PCR (LAM-PCR). Nat Methods *4*, 1051-1057.
745 10.1038/nmeth1103.
746 13. Paruzynski, A., Arens, A., Gabriel, R., Bartholomae, C.C., Scholz, S., Wang, W., Wolf,
747 S., Glimm, H., Schmidt, M., and von Kalle, C. (2010). Genome-wide high-throughput
748 integrome analyses by nrLAM-PCR and next-generation sequencing. Nat Protoc *5*, 1379-
749 1395. 10.1038/nprot.2010.87.

750 14. Zhong, L., Malani, N., Li, M., Brady, T., Xie, J., Bell, P., Li, S., Jones, H., Wilson, J.M.,
751 Flotte, T.R., et al. (2013). Recombinant adeno-associated virus integration sites in murine
752 liver after ornithine transcarbamylase gene correction. Hum Gene Ther *24*, 520-525.
753 10.1089/hum.2012.112.
754 15. Cogne, B., Snyder, R., Lindenbaum, P., Dupont, J.B., Redon, R., Moullier, P., and Leger,
755 A. (2014). NGS library preparation may generate artifactual integration sites of AAV
756 vectors. Nat Med *20*, 577-578. 10.1038/nm.3578.
757 16. Sunshine, S., Kirchner, R., Amr, S.S., Mansur, L., Shakhbatyan, R., Kim, M., Bosque,
758 A., Siliciano, R.F., Planelles, V., Hofmann, O., et al. (2016). HIV Integration Site
759 Analysis of Cellular Models of HIV Latency with a Probe-Enriched Next-Generation
760 Sequencing Assay. J Virol *90*, 4511-4519. 10.1128/JVI.01617-15.
761 17. Sun, C., Liu, L., Perez, L., Li, X., Liu, Y., Xu, P., Boritz, E.A., Mullins, J.I., and Abate,
762 A.R. (2022). Droplet-microfluidics-assisted sequencing of HIV proviruses and their
763 integration sites in cells from people on antiretroviral therapy. Nat Biomed Eng.
764 10.1038/s41551-022-00864-8.
765 18. Wang, W., Fasolino, M., Cattau, B., Goldman, N., Kong, W., Frederick, M.A., McCright,
766 S.J., Kiani, K., Fraietta, J.A., and Vahedi, G. (2020). Joint profiling of chromatin
767 accessibility and CAR-T integration site analysis at population and single-cell levels.
768 Proc Natl Acad Sci U S A *117*, 5442-5452. 10.1073/pnas.1919259117.
769 19. Oziolor, E.M., Kumpf, S.W., Qian, J., Gosink, M., Sheehan, M., Rubitski, D.M.,
770 Newman, L., Whiteley, L.O., and Lanz, T.A. (2023). Comparing molecular and
771 computational approaches for detecting viral integration of AAV gene therapy constructs.
772 Mol Ther Methods Clin Dev *29*, 395-405. 10.1016/j.omtm.2023.04.009.
773 20. Yu, J.J., Wu, T.L., Liszewski, M.K., Dai, J., Swiggard, W.J., Baytop, C., Frank, I.,
774 Levine, B.L., Yang, W., Theodosopoulos, T., and O'Doherty, U. (2008). A more precise
775 HIV integration assay designed to detect small differences finds lower levels of
776 integrated DNA in HAART treated patients. Virology *379*, 78-86.
777 10.1016/j.virol.2008.05.030.
778 21. Cesana, D., Calabria, A., Rudilosso, L., Gallina, P., Benedicenti, F., Spinozzi, G.,
779 Schiroli, G., Magnani, A., Acquati, S., Fumagalli, F., et al. (2021). Retrieval of vector
780 integration sites from cell-free DNA. Nat Med *27*, 1458-1470. 10.1038/s41591-021-
781 01389-4.
782 22. Chen, H.M., Resendes, R., Ghodssi, A., Sookiasian, D., Tian, M., Dollive, S., Adamson-
783 Small, L., Avila, N., Tazearslan, C., Thompson, J.F., et al. (2020). Molecular
784 characterization of precise in vivo targeted gene integration in human cells using
785 AAVHSC15. PLoS One *15*, e0233373. 10.1371/journal.pone.0233373.
786 23. Wells, D.W., Guo, S., Shao, W., Bale, M.J., Coffin, J.M., Hughes, S.H., and Wu, X.
787 (2020). An analytical pipeline for identifying and mapping the integration sites of HIV
788 and other retroviruses. BMC Genomics *21*, 216. 10.1186/s12864-020-6647-4.
789 24. Ahmed, S.S., Rubin, H., Wang, M., Faulkner, D., Sengooba, A., Dollive, S.N., Avila, N.,
790 Ellsworth, J.L., Lamppu, D., Lobikin, M., et al. (2020). Sustained Correction of a Murine
791 Model of Phenylketonuria following a Single Intravenous Administration of
792 AAVHSC15-PAH. Mol Ther Methods Clin Dev *17*, 568-580.
793 10.1016/j.omtm.2020.03.009.
794 25. Duan, D., Sharma, P., Yang, J., Yue, Y., Dudus, L., Zhang, Y., Fisher, K.J., and
795 Engelhardt, J.F. (1998). Circular intermediates of recombinant adeno-associated virus

796 have defined structural characteristics responsible for long-term episomal persistence in
797 muscle tissue. J Virol *72*, 8568-8577. 10.1128/JVI.72.11.8568-8577.1998.
798 26. Azuma, H., Paulk, N., Ranade, A., Dorrell, C., Al-Dhalimy, M., Ellis, E., Strom, S., Kay,
799 M.A., Finegold, M., and Grompe, M. (2007). Robust expansion of human hepatocytes in
800 Fah-/-/Rag2-/-/Il2rg-/- mice. Nat Biotechnol *25*, 903-910. 10.1038/nbt1326.
801 27. Hsu, P.D., Scott, D.A., Weinstein, J.A., Ran, F.A., Konermann, S., Agarwala, V., Li, Y.,
802 Fine, E.J., Wu, X., Shalem, O., et al. (2013). DNA targeting specificity of RNA-guided
803 Cas9 nucleases. Nat Biotechnol *31*, 827-832. 10.1038/nbt.2647.
804 28. Sherman, E., Nobles, C., Berry, C.C., Six, E., Wu, Y., Dryga, A., Malani, N., Male, F.,
805 Reddy, S., Bailey, A., et al. (2017). INSPIIRED: A Pipeline for Quantitative Analysis of
806 Sites of New DNA Integration in Cellular Genomes. Mol Ther Methods Clin Dev *4*, 39-
807 49. 10.1016/j.omtm.2016.11.002.
808 29. Prout, J., Tian, M., Palladino, A., Wright, J., and Thompson, J.F. (2023). LNA blockers
809 for improved amplification selectivity. Sci Rep *13*, 4858. 10.1038/s41598-023-31871-7.
810 30. Yin, P.H., Lee, H.C., Chau, G.Y., Wu, Y.T., Li, S.H., Lui, W.Y., Wei, Y.H., Liu, T.Y.,
811 and Chi, C.W. (2004). Alteration of the copy number and deletion of mitochondrial DNA
812 in human hepatocellular carcinoma. Br J Cancer *90*, 2390-2396. 10.1038/sj.bjc.6601838.
813 31. Chen, Y.S., Lu, S., Zhang, B., Du, T., Li, W.J., Lei, M., Zhou, Y., Zhang, Y., Liu, P.,
814 Sun, Y.Q., et al. (2022). Comprehensive analysis of RNA-seq and whole genome
815 sequencing data reveals no evidence for SARS-CoV-2 integrating into host genome.
816 Protein Cell *13*, 379-385. 10.1007/s13238-021-00861-8.
817 32. Smits, N., Rasmussen, J., Bodea, G.O., Amarilla, A.A., Gerdes, P., Sanchez-Luque, F.J.,
818 Ajjikuttira, P., Modhiran, N., Liang, B., Faivre, J., et al. (2021). No evidence of human
819 genome integration of SARS-CoV-2 found by long-read DNA sequencing. Cell Rep *36*,
820 109530. 10.1016/j.celrep.2021.109530.
821 33. Soares, L.M.M.H., Terrence ; Selby, Donald E. ; Adjei, Samuel; Wang, Wei; Thompson,
822 John F. (2022). Quantitative DNA estimation using single-molecule, long-read
823 sequencing. In review.
824 34. Nathwani, A.C. (2019). Gene therapy for hemophilia. Hematology Am Soc Hematol
825 Educ Program *2019*, 1-8. 10.1182/hematology.2019000007.
826 35. George, L.A., Monahan, P.E., Eyster, M.E., Sullivan, S.K., Ragni, M.V., Croteau, S.E.,
827 Rasko, J.E.J., Recht, M., Samelson-Jones, B.J., MacDougall, A., et al. (2021). Multiyear
828 Factor VIII Expression after AAV Gene Transfer for Hemophilia A. N Engl J Med *385*,
829 1961-1973. 10.1056/NEJMoa2104205.
830 36. Villiger, L., Grisch-Chan, H.M., Lindsay, H., Ringnalda, F., Pogliano, C.B., Allegri, G.,
831 Fingerhut, R., Haberle, J., Matos, J., Robinson, M.D., et al. (2018). Treatment of a
832 metabolic liver disease by in vivo genome base editing in adult mice. Nat Med *24*, 1519-
833 1525. 10.1038/s41591-018-0209-1.
834 37. Richards, D.Y., Winn, S.R., Dudley, S., Nygaard, S., Mighell, T.L., Grompe, M., and
835 Harding, C.O. (2020). AAV-Mediated CRISPR/Cas9 Gene Editing in Murine
836 Phenylketonuria. Mol Ther Methods Clin Dev *17*, 234-245. 10.1016/j.omtm.2019.12.004.
837 38. Bock, D., Rothgangl, T., Villiger, L., Schmidheini, L., Matsushita, M., Mathis, N.,
838 Ioannidi, E., Rimann, N., Grisch-Chan, H.M., Kreutzer, S., et al. (2022). In vivo prime
839 editing of a metabolic liver disease in mice. Sci Transl Med *14*, eabl9238.
840 10.1126/scitranslmed.abl9238.

841 39. Hoijer, I., Emmanouilidou, A., Ostlund, R., van Schendel, R., Bozorgpana, S.,
842 Tijsterman, M., Feuk, L., Gyllensten, U., den Hoed, M., and Ameur, A. (2022). CRISPR-
843 Cas9 induces large structural variants at on-target and off-target sites in vivo that
844 segregate across generations. Nat Commun *13*, 627. 10.1038/s41467-022-28244-5.
845 40. Aquino-Jarquin, G. (2021). Current advances in overcoming obstacles of CRISPR/Cas9
846 off-target genome editing. Mol Genet Metab *134*, 77-86. 10.1016/j.ymgme.2021.08.002.
847 41. Kaeppel, C., Beattie, S.G., Fronza, R., van Logtenstein, R., Salmon, F., Schmidt, S.,
848 Wolf, S., Nowrouzi, A., Glimm, H., von Kalle, C., et al. (2013). A largely random AAV
849 integration profile after LPLD gene therapy. Nat Med *19*, 889-891. 10.1038/nm.3230.
850 42. Nguyen, G.N., Everett, J.K., Kafle, S., Roche, A.M., Raymond, H.E., Leiby, J., Wood,
851 C., Assenmacher, C.A., Merricks, E.P., Long, C.T., et al. (2021). A long-term study of
852 AAV gene therapy in dogs with hemophilia A identifies clonal expansions of transduced
853 liver cells. Nat Biotechnol *39*, 47-55. 10.1038/s41587-020-0741-7.
854 43. Gil-Farina, I., Fronza, R., Kaeppel, C., Lopez-Franco, E., Ferreira, V., D'Avola, D.,
855 Benito, A., Prieto, J., Petry, H., Gonzalez-Aseguinolaza, G., and Schmidt, M. (2016).
856 Recombinant AAV Integration Is Not Associated With Hepatic Genotoxicity in
857 Nonhuman Primates and Patients. Mol Ther *24*, 1100-1105. 10.1038/mt.2016.52.
858 44. Strom, S.C., Davila, J., and Grompe, M. (2010). Chimeric mice with humanized liver:
859 tools for the study of drug metabolism, excretion, and toxicity. Methods Mol Biol *640*,
860 491-509. 10.1007/978-1-60761-688-7_27.
861 45. Gualdron-Lopez, M., Flannery, E.L., Kangwanrangsan, N., Chuenchob, V., Fernandez-
862 Orth, D., Segui-Barber, J., Royo, F., Falcon-Perez, J.M., Fernandez-Becerra, C., Lacerda,
863 M.V.G., et al. (2018). Characterization of Plasmodium vivax Proteins in Plasma-Derived
864 Exosomes From Malaria-Infected Liver-Chimeric Humanized Mice. Front Microbiol *9*,
865 1271. 10.3389/fmicb.2018.01271.
866 46. Minniti, M.E., Pedrelli, M., Vedin, L.L., Delbes, A.S., Denis, R.G.P., Oorni, K., Sala, C.,
867 Pirazzini, C., Thiagarajan, D., Nurmi, H.J., et al. (2020). Insights From Liver-Humanized
868 Mice on Cholesterol Lipoprotein Metabolism and LXR-Agonist Pharmacodynamics in
869 Humans. Hepatology *72*, 656-670. 10.1002/hep.31052.
870 47. Westhaus, A., Cabanes-Creus, M., Rybicki, A., Baltazar, G., Navarro, R.G., Zhu, E.,
871 Drouyer, M., Knight, M., Albu, R.F., Ng, B.H., et al. (2020). High-Throughput In Vitro,
872 Ex Vivo, and In Vivo Screen of Adeno-Associated Virus Vectors Based on Physical and
873 Functional Transduction. Hum Gene Ther *31*, 575-589. 10.1089/hum.2019.264.
874 48. Naugler, W.E., Tarlow, B.D., Fedorov, L.M., Taylor, M., Pelz, C., Li, B., Darnell, J., and
875 Grompe, M. (2015). Fibroblast Growth Factor Signaling Controls Liver Size in Mice
876 With Humanized Livers. Gastroenterology *149*, 728-740 e715.
877 10.1053/j.gastro.2015.05.043.
878 49. Graham, T., McIntosh, J., Work, L.M., Nathwani, A., and Baker, A.H. (2008).
879 Performance of AAV8 vectors expressing human factor IX from a hepatic-selective
880 promoter following intravenous injection into rats. Genet Vaccines Ther *6*, 9.
881 10.1186/1479-0556-6-9.

882

Table 1: Limit of Blank using control DNA spikes in control genomic DNA

A) Samples with non-homologous transduced vector and no spike of lysed vector or A11 positive control

Animal	HuLiv	Mouse
Vector	ms006	GT_DnG
A11 Positive control DNA	0	0
Total Reads	4,026,791	934,594
Usable Reads	4,019,615	932,035
Reads mapping to RHA	800,530	73,215
Reads mapping to both RHA and hg38	2,752	1,411
Reads after removal of incorrect vector sequences	2,683	63
Reads with coPAH and RHA and additional sequence	683	10
Reads with coPAH, RHA, and hg38	589	6
Reads with coPAH, RHA, with hg38 within 30 bp	211	3
Reads after removal of PCR duplicates	20	3
A11 Reads (based on SNPs)	0	0
Off Targets Called (read depth 1)	5	3
Off Targets Called (read depth 3)	1	0

B) Samples with lysed vector DNA spike

Genomic DNA (1 µg)	Mouse	Human	Human	Human	Human	Human	Human	Human	Human	Human
Lysed Vector	3E+08	3E+08	3E+07	3E+06	3E+06	3E+06	3E+06	3E+06	3E+06	3E+06
A11 Positive control DNA	0	0	0	0	5%	2.5%	2.5%	1%	0.5%	0.1%
Total Reads	4,862,671	3,666,249	3,016,978	3,531,039	254,365	160,075	416,798	485,866	958,306	937,532
Usable Reads	4,845,887	3,657,311	3,012,807	3,525,640	253,488	152,919	413,728	485,163	953,340	933,572
Reads mapping to RHA	71,111	7,201	17,365	359,507	3,705	14,442	31,448	58,157	716,577	637,402
Reads mapping to both RHA and hg38	5	2	15	2,175	387	328	1,738	1,507	3,972	3,668
Reads after removal of incorrect vector sequences	4	1	14	587	350	324	1,671	1,467	3,859	3,571
Reads with coPAH and RHA and additional sequence	1	0	4	94	35	30	189	282	995	686
Reads with coPAH, RHA, and hg38	1	0	4	71	33	21	160	242	871	568
Reads with coPAH, RHA, with hg38 within 30 bp	0	0	3	3	13	9	82	60	264	12
Reads after removal of PCR duplicates	0	0	3	3	10	9	34	23	43	12
A11 Reads (based on SNPs)	0	0	0	0	9	9	31	1	1	0
Off Targets Called (read depth 1)	0	0	1	3	0	0	1	8	14	12
Off Targets Called (read depth 3)	0	0	0	0	0	0	0	1	1	0